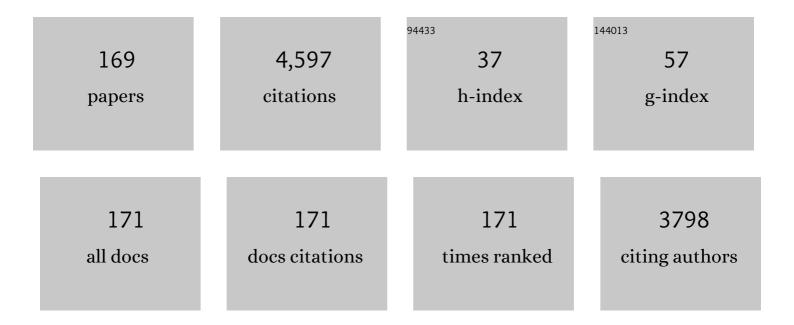
Yi Zhang

List of Publications by Year in descending order

Source: https://exaly.com/author-pdf/1956295/publications.pdf Version: 2024-02-01



<u>ΥΙ ΖΗΛΝΟ</u>

#	Article	IF	CITATIONS
1	Li+ doping induced zero-thermal quenching in Cs3Zn6––B9O21:xEu3+,yLi+ (0 ≤ ≤0.10, 0.06 ≤9 â% Journal of Rare Earths, 2023, 41, 1478-1486.	₀¤0,16). 4.8	1
2	Interfacial Engineering of Wideâ€Bandgap Perovskites for Efficient Perovskite/CZTSSe Tandem Solar Cells. Advanced Functional Materials, 2022, 32, 2107359.	14.9	43
3	Optimization of the Selenization Pressure Enabling Efficient Cu ₂ ZnSn(S,Se) ₄ Solar Cells. Solar Rrl, 2022, 6, .	5.8	8
4	Efficiency improvement of electrodeposition-processed Cu(In,Ga)Se2 solar cell with widen surface bandgap by spin-coating In2S3 thin film. Applied Surface Science, 2022, 578, 152063.	6.1	7
5	Band-gap-graded Cu ₂ ZnSn(S,Se) ₄ drives highly efficient solar cells. Energy and Environmental Science, 2022, 15, 693-704.	30.8	74
6	Interface Etching Leads to the Inversion of the Conduction Band Offset between the CdS/Sb ₂ Se ₃ Heterojunction and High-Efficient Sb ₂ Se ₃ Solar Cells. ACS Applied Energy Materials, 2022, 5, 2531-2541.	5.1	18
7	Oxygen vacancy content drives self-reduction and anti-thermal quenching. Journal of Materials Chemistry C, 2022, 10, 4317-4326.	5.5	20
8	Intense Luminescence and Good Thermal Stability in a Mn ²⁺ -Activated Mg-Based Phosphor with Self-Reduction. Inorganic Chemistry, 2022, 61, 5495-5501.	4.0	13
9	Interface Modification Uncovers the Potential Application of SnO ₂ /TiO ₂ Double Electron Transport Layer in Efficient Cadmiumâ€Free Sb ₂ Se ₃ Devices. Advanced Materials Interfaces, 2022, 9, .	3.7	14
10	Al-doped ZnO thin films with excellent optoelectronic properties prepared using H2-assisted reactive magnetron sputtering at low temperatures for potential application in photovoltaic devices. Journal of Materials Science: Materials in Electronics, 2022, 33, 10267-10277.	2.2	1
11	Double interface modification promotes efficient Sb2Se3 solar cell by tailoring band alignment and light harvest. Journal of Energy Chemistry, 2022, 70, 191-200.	12.9	11
12	Wide bandgap CIGS thin films via Ag-PDT to ameliorate the interface quality of CIGS/CdS heterojunction. Journal of Materials Science: Materials in Electronics, 2022, 33, 11055.	2.2	1
13	Tuning the Work Function of the Metal Back Contact toward Efficient Cu ₂ ZnSnSe ₄ Solar Cells. Solar Rrl, 2021, 5, .	5.8	13
14	Promising Cd-free double buffer layer in CZTSSe thin film solar cells. Science China Materials, 2021, 64, 288-295.	6.3	16
15	A promising photovoltaic material Cu2MnSn(S,Se)4: Film growth and its application in solar cell. Solar Energy Materials and Solar Cells, 2021, 219, 110788.	6.2	9
16	Effect of Cu content in CIGSe absorber on MoSe2 formation during post-selenization process. Materials Science in Semiconductor Processing, 2021, 121, 105275.	4.0	6
17	Pulsed rapid thermal process for tailoring the surface sulfurization of CICSe thin film at low temperature. Solar Energy Materials and Solar Cells, 2021, 221, 110871.	6.2	2
18	Role of Intrinsic Surface States in Efficiency Attenuation of GaNâ€Based Microâ€Lightâ€Emittingâ€Diodes. Physica Status Solidi - Rapid Research Letters, 2021, 15, 2000487.	2.4	18

#	Article	IF	CITATIONS
19	Back contact modification of the optoelectronic device with transition metal dichalcogenide VSe2 film drives solar cell efficiency. Journal of Materiomics, 2021, 7, 470-477.	5.7	10
20	Na-doping-induced modification of the Cu2ZnSn(S,Se)4/CdS heterojunction towards efficient solar cells. Journal of Energy Chemistry, 2021, 57, 618-626.	12.9	32
21	Intrinsic and extrinsic defects build a novel mechanoluminescent phosphor Na ₂ MgGeO ₄ :Mn ²⁺ . Journal of Materials Chemistry C, 2021, 9, 3513-3521.	5.5	28
22	Construction of a novel mechanoluminescent phosphor Li ₂ MgGeO ₄ : <i>x</i> Mn ²⁺ by defect control. Dalton Transactions, 2021, 50, 8803-8810.	3.3	16
23	Defects and Surface Electrical Property Transformation Induced by Elemental Interdiffusion at the p–n Heterojunction via High-Temperature Annealing. ACS Applied Materials & Interfaces, 2021, 13, 12211-12220.	8.0	25
24	Enhancing Surface Properties for Electrodeposited Cu(In,Ga)Se ₂ Films by (NH ₄) ₂ S Solution at Room Temperature. ACS Applied Energy Materials, 2021, 4, 3822-3831.	5.1	7
25	Boosting V _{OC} of antimony chalcogenide solar cells: A review on interfaces and defects. Nano Select, 2021, 2, 1818-1848.	3.7	66
26	Defect Control for Highâ€Efficiency Cu ₂ ZnSn(S,Se) ₄ Solar Cells by Atomic Layer Deposition of Al ₂ O ₃ on Precursor Film. Solar Rrl, 2021, 5, 2100181.	5.8	21
27	New Solution-Processed Surface Treatment to Improve the Photovoltaic Properties of Electrodeposited Cu(In,Ga)Se ₂ (CIGSe) Solar Cells. ACS Applied Materials & Interfaces, 2021, 13, 25451-25460.	8.0	5
28	Oxygen Promotes the Formation of MoSe ₂ at the Interface of Cu ₂ ZnSnSe ₄ /Mo. Journal of Physical Chemistry Letters, 2021, 12, 4447-4452.	4.6	8
29	Defectâ€Induced Selfâ€Reduction and Antiâ€Thermal Quenching in NaZn(PO ₃) ₃ :Mn ²⁺ Red Phosphor. Advanced Optical Materials, 2021, 9, 2100870.	7.3	69
30	Effect of MoS2 interlayer on performances of copper-barium-tin-sulfur thin film solar cells via theoretical simulation. Solar Energy, 2021, 223, 384-397.	6.1	15
31	Pulse Selenization in Cu(In,Ga)Se2 Solar Cells: A Promising Approach to Achieve High Efficiency by Electrodeposition. ACS Applied Energy Materials, 2021, 4, 8322-8329.	5.1	1
32	Band alignment tuning at Mo/CZTS back contact interface through surface oxidation states control of Mo substrate. Solar Energy Materials and Solar Cells, 2021, 229, 111141.	6.2	9
33	Enhancing the Photovoltaic Performance of Cu ₂ ZnSn(S,Se) ₄ Solar Cells with Ba Trace Doping: Large Chemical Mismatch Cation Incorporation. Solar Rrl, 2021, 5, 2100607.	5.8	7
34	High-efficiency ultra-thin Cu2ZnSnS4 solar cells by double-pressure sputtering with spark plasma sintered quaternary target. Journal of Energy Chemistry, 2021, 61, 186-194.	12.9	20
35	Li2S doping into CZTSe drives the large improvement of VOC of solar cell. Journal of Energy Chemistry, 2021, 62, 637-644.	12.9	15
36	Nâ€īype Surface Design for pâ€īype CZTSSe Thin Film to Attain High Efficiency. Advanced Materials, 2021, 33, e2104330.	21.0	49

#	Article	IF	CITATIONS
37	Investigation on the Structure and Morphology of CZTSe Solar Cells by Adjusting Cu–Ge Buffer Layers. ACS Applied Energy Materials, 2021, 4, 11793-11801.	5.1	6
38	Remarkable Sb ₂ Se ₃ Solar Cell with a Carbon Electrode by Tailoring Film Growth during the VTD Process. ACS Applied Energy Materials, 2021, 4, 13335-13346.	5.1	20
39	Remarkable Cd-free Sb ₂ Se ₃ solar cell yield achieved by interface band-alignment and growth orientation screening. Journal of Materials Chemistry A, 2021, 9, 26963-26975.	10.3	17
40	Self-Reduction-Related Defects, Long Afterglow, and Mechanoluminescence in Centrosymmetric Li ₂ ZnGeO ₄ :Mn ²⁺ . Inorganic Chemistry, 2021, 60, 18432-18441.	4.0	33
41	An efficient Li ⁺ -doping strategy to optimize the band alignment of a Cu ₂ ZnSn(S,Se) ₄ /CdS interface by a Se&LiF co-selenization process. Journal of Materials Chemistry A, 2020, 8, 22065-22074.	10.3	51
42	Advances in kesterite Cu2ZnSn(S, Se)4 solar cells. Science Bulletin, 2020, 65, 698-701.	9.0	49
43	Efficiency Enhancement of CICS Solar Cells via Recombination Passivation. ACS Applied Energy Materials, 2020, 3, 9459-9467.	5.1	13
44	A Novel Metal Precursor Structure for Electrodepositing Ultrathin CICSe Thin-Film Solar Cell with High Efficiency. ACS Applied Materials & Interfaces, 2020, 12, 24403-24410.	8.0	14
45	Nanoscale Surface Electrical Properties Tailored by Roomâ€Temperature Sulfurization for Highâ€Efficient CZTSe Solar Cells. Advanced Materials Interfaces, 2020, 7, 2000564.	3.7	15
46	Over 10% Efficient Pure CZTSe Solar Cell Fabricated by Electrodeposition with Ge Doping. Solar Rrl, 2020, 4, 2000059.	5.8	27
47	Recent Progress on Cu 2 BaSn(S x Se 1– x) 4 : From Material to Solar Cell Applications. Physica Status Solidi (A) Applications and Materials Science, 2020, 217, 2000060.	1.8	4
48	Intense green elastico-mechanoluminescence from KZn(PO3)3:Tb3+. Applied Physics Letters, 2020, 116, .	3.3	14
49	Interstitial oxygen defect induced mechanoluminescence in KCa(PO ₃) ₃ :Mn ²⁺ . Journal of Materials Chemistry C, 2020, 8, 6587-6594.	5.5	25
50	Current improvement in substrate structured Sb2S3 solar cells with MoSe2 interlayer. Chinese Physics B, 2020, 29, 058801.	1.4	6
51	10.1063/1.5134712.1., 2020,,.		0
52	Electrodeposition of Cu thin film assisted by Cu nanoparticles for Cu2ZnSnSe4 solar cell applications. Applied Physics A: Materials Science and Processing, 2019, 125, 1.	2.3	3
53	Engineering CIGS grains qualities to achieve high efficiency in ultrathin Cu(In Ga1â~')Se2 solar cells with a single-gradient band gap profile. Results in Physics, 2019, 12, 704-711.	4.1	37
54	Reactive Mechanism of Cu2ZnSnSe4 Thin Films Prepared by Reactive Annealing of the Cu/Zn Metal Layer in a SnSex + Se Atmosphere. Crystals, 2019, 9, 10.	2.2	14

#	Article	IF	CITATIONS
55	Two-step growth of VSe ₂ films and their photoelectric properties*. Chinese Physics B, 2019, 28, 058101.	1.4	8
56	Coexistence of self-reduction from Mn ⁴⁺ to Mn ²⁺ and elastico-mechanoluminescence in diphase KZn(PO ₃) ₃ :Mn ²⁺ . Journal of Materials Chemistry C, 2019, 7, 7096-7103.	5.5	43
57	Optimizing the thickness of sputtering-Zn(O, S) buffer layer for all-dry Cd-free CIGS solar cells. Materials Research Express, 2019, 6, 086431.	1.6	8
58	Synergistic effect of Na and Se on CZTSe solar cells through a soft chemical process. Solar Energy Materials and Solar Cells, 2019, 198, 35-43.	6.2	20
59	Insight into band alignment of Zn(O,S)/CZTSe solar cell by simulation. Chinese Physics B, 2019, 28, 048801.	1.4	9
60	Formation of the front-gradient bandgap in the Ag doped CZTSe thin films and solar cells. Journal of Energy Chemistry, 2019, 35, 188-196.	12.9	35
61	Substrate structured Sb2S3 thin film solar cells fabricated by rapid thermal evaporation method. Solar Energy, 2019, 182, 64-71.	6.1	49
62	Over 6% Certified Sb ₂ (S,Se) ₃ Solar Cells Fabricated via In Situ Hydrothermal Growth and Postselenization. Advanced Electronic Materials, 2019, 5, 1800683.	5.1	78
63	Roomâ€Temperature Surface Sulfurization for Highâ€Performance Kesterite CZTSe Solar Cells. Solar Rrl, 2019, 3, 1800236.	5.8	21
64	Lowâ€Temperature Growth of Submicron Cu(In, Ga)Se ₂ Solar Cells Based on Molybdenum Oxide Back Interface Layer. Physica Status Solidi (A) Applications and Materials Science, 2019, 216, 1800378.	1.8	1
65	Hole-selective NiO:Cu contact for NiO/Si heterojunction solar cells. Journal of Alloys and Compounds, 2018, 747, 563-570.	5.5	38
66	Insight into the role of post-annealing in air for high efficient Cu2ZnSn(S,Se)4 solar cells. Solar Energy Materials and Solar Cells, 2018, 182, 228-236.	6.2	37
67	A Precursor Stacking Strategy to Boost Open-Circuit Voltage of Cu ₂ ZnSnS ₄ Thin-Film Solar Cells. IEEE Journal of Photovoltaics, 2018, 8, 856-863.	2.5	13
68	Interfaces of high-efficiency kesterite Cu 2 ZnSnS(e) 4 thin film solar cells. Chinese Physics B, 2018, 27, 018803.	1.4	48
69	Artificial twin-layer configurations of Zn(O,S) films by radio frequency sputtering in all dry processed eco-friendly Cu(In,Ca)Se ₂ solar cells. Journal Physics D: Applied Physics, 2018, 51, 105502.	2.8	0
70	Cation Substitution in Earthâ€Abundant Kesterite Photovoltaic Materials. Advanced Science, 2018, 5, 1700744.	11.2	161
71	Thinâ€Film Solar Cells: Cation Substitution in Earthâ€Abundant Kesterite Photovoltaic Materials (Adv. Sci.) Tj ETÇ	q]10.78	4314 rgBT

⁷² Influence of Cu on Ga diffusion during post-selenizing the electrodeposited Cu/In/Ga metallic precursor process. Solar Energy Materials and Solar Cells, 2018, 182, 92-97.

6.2 11

#	Article	IF	CITATIONS
73	Path towards high-efficient kesterite solar cells. Journal of Energy Chemistry, 2018, 27, 1040-1053.	12.9	68
74	Adjustment of alkali element incorporations in Cu(In,Ga)Se2 thin films with wet chemistry Mo oxide as a hosting reservoir. Solar Energy Materials and Solar Cells, 2018, 174, 16-24.	6.2	28
75	Tailoring Mo(S,Se)2 structure for high efficient Cu2ZnSn(S,Se)4 solar cells. Solar Energy Materials and Solar Cells, 2018, 176, 302-309.	6.2	37
76	Modified Back Contact Interface of CZTSe Thin Film Solar Cells: Elimination of Double Layer Distribution in Absorber Layer. Advanced Science, 2018, 5, 1700645.	11.2	51
77	Modifying the Hetero-junction Interface of Cu <inf>2</inf> ZnSnSe <inf>4</inf> Solar Cells. , 2018, , .		0
78	Morphology Modification of Sn and Zn Metal Thin Films Applied for CZTSe Solar Cell: the Effect of Pulse Current Electrodeposition. , 2018, , .		1
79	Promising Sb ₂ (S,Se) ₃ Solar Cells with High Open Voltage by Application of a TiO ₂ /CdS Double Buffer Layer. Solar Rrl, 2018, 2, 1800208.	5.8	83
80	Efficient Optimization of the Performance of Mn ²⁺ â€Doped Kesterite Solar Cell: Machine Learning Aided Synthesis of High Efficient Cu ₂ (Mn,Zn)Sn(S,Se) ₄ Solar Cells. Solar Rrl, 2018, 2, 1800198.	5.8	46
81	Modified crystal quality of Cu(In,Ga)Se2 solar cells: Elimination of island-shaped indium layer by pulse current electrodeposition method. Journal of Alloys and Compounds, 2018, 766, 178-185.	5.5	6
82	Analysis of the structure and abnormal photoluminescence of a red-emitting LiMgBO ₃ :Mn ²⁺ phosphor. Dalton Transactions, 2018, 47, 13094-13105.	3.3	20
83	Band bending near grain boundaries of Cu2ZnSn(S,Se)4 thin films and its effect on photovoltaic performance. Nano Energy, 2018, 51, 37-44.	16.0	30
84	Improvement of the recombination and infrared light losses by rear surface chemical polishing in silicon heterojunction solar cells. Applied Physics A: Materials Science and Processing, 2017, 123, 1.	2.3	5
85	Controllable Growth of Ga Film Electrodeposited from Aqueous Solution and Cu(In,Ga)Se ₂ Solar Cells. ACS Applied Materials & Interfaces, 2017, 9, 18682-18690.	8.0	21
86	Sm ³⁺ and Eu ³⁺ codoped SrBi ₂ B ₂ O ₇ : a red-emitting phosphor with improved thermal stability. RSC Advances, 2017, 7, 1146-1153.	3.6	43
87	Restraining the Band Fluctuation of CBDâ€Zn(O,S) Layer: Modifying the Heteroâ€Junction Interface for High Performance Cu ₂ ZnSnSe ₄ Solar Cells With Cdâ€Free Buffer Layer. Solar Rrl, 2017, 1, 1700075.	5.8	29
88	Effect of different thermo-treatment at relatively low temperatures on the properties of indium‑tin-oxide thin films. Thin Solid Films, 2017, 636, 702-709.	1.8	16
89	Tailoring the defects and carrier density for beyond 10% efficient CZTSe thin film solar cells. Solar Energy Materials and Solar Cells, 2017, 159, 447-455.	6.2	129
90	Energy transfer between Ce^3+ and Tb^3+ and the enhanced luminescence of a green phosphor SrB_2O_4:Ce^3+, Tb^3+, Na^+. Optical Materials Express, 2016, 6, 1172.	3.0	20

#	Article	IF	CITATIONS
91	Synthesis and performance of Cu2ZnSnS4 semiconductor as photocathode for solar water splitting. Journal of Alloys and Compounds, 2016, 688, 923-932.	5.5	38
92	Growth of Cu ₂ ZnSnSe ₄ Film under Controllable Se Vapor Composition and Impact of Low Cu Content on Solar Cell Efficiency. ACS Applied Materials & Interfaces, 2016, 8, 10283-10292.	8.0	65
93	Pulse electro-deposition of copper on molybdenum for Cu(In,Ga)Se2 and Cu2ZnSnSe4 solar cell applications. Journal of Power Sources, 2016, 326, 211-219.	7.8	36
94	Crystal Structure of High-Temperature Phase β-NaSrBO ₃ and Photoluminescence of β-NaSrBO ₃ :Ce ³⁺ . Inorganic Chemistry, 2016, 55, 6487-6495.	4.0	25
95	10% Efficiency Cu2ZnSn(S,Se)4 thin film solar cells fabricated by magnetron sputtering with enlarged depletion region width. Solar Energy Materials and Solar Cells, 2016, 149, 242-249.	6.2	153
96	Comparative study of the role of Ga in CIGS solar cells with different thickness. Thin Solid Films, 2016, 598, 189-194.	1.8	13
97	The influence of pre-heating temperature on the CIGS thin film growth and device performance prepared in cracked-Se atmosphere. Semiconductor Science and Technology, 2015, 30, 105012.	2.0	7
98	Barrier effect of AlN film in flexible Cu(In,Ga)Se2 solar cells on stainless steel foil and solar cell. Journal of Alloys and Compounds, 2015, 627, 1-6.	5.5	21
99	A Temporary Barrier Effect of the Alloy Layer During Selenization: Tailoring the Thickness of MoSe ₂ for Efficient Cu ₂ ZnSnSe ₄ Solar Cells. Advanced Energy Materials, 2015, 5, 1402178.	19.5	137
100	Effects of metal ion concentration on electrodeposited CuZnSn film and its application in kesterite Cu ₂ ZnSnS ₄ solar cells. RSC Advances, 2015, 5, 65114-65122.	3.6	23
101	The influence of cracked selenium flux on CIGS thin film growth and device performance prepared by two-step selenization processes. Solar Energy Materials and Solar Cells, 2015, 139, 108-114.	6.2	27
102	Carbon concentration dependent grain growth of Cu ₂ ZnSnS ₄ thin films. RSC Advances, 2015, 5, 20178-20185.	3.6	37
103	Modified co-evaporation process for fabrication of 4 cm × 4 cm large area flexible CIGS thin film solar cells on polyimide substrate. Materials Research Express, 2015, 2, 046403.	1.6	8
104	Structure refinement and one-center luminescence of Eu3+ activated ZnBi2B2O7 under UV excitation. Journal of Alloys and Compounds, 2015, 648, 500-506.	5.5	10
105	Abnormal luminescent property of Mn ²⁺ in α-LiZnBO ₃ :Mn ²⁺ . Dalton Transactions, 2015, 44, 1427-1434.	3.3	27
106	On the growth process of Cu2ZnSn(S,Se)4 absorber layer formed by selenizing Cu–ZnS–SnS precursors and its photovoltaic performance. Solar Energy Materials and Solar Cells, 2015, 132, 363-371.	6.2	45
107	Site occupancy and photoluminescence of Sm^3+ in KSr_4(BO_3)_3:Sm^3+ phosphors. Optical Materials Express, 2014, 4, 1535.	3.0	37
108	Site occupancy and photoluminescence properties of Eu ³⁺ -activated Ba ₂ ZnB ₂ O ₆ phosphor. RSC Advances, 2014, 4, 64244-64251.	3.6	35

#	Article	IF	CITATIONS
109	The effects of sodium on the growth of Cu(In,Ga)Se ₂ thin films using low-temperature three-stage process on polyimide substrate. Journal Physics D: Applied Physics, 2014, 47, 045105.	2.8	6
110	Impact of the Electronâ€Transport Layer on the Performance of Solutionâ€Processed Smallâ€Molecule Organic Solar Cells. ChemSusChem, 2014, 7, 2358-2364.	6.8	40
111	Structure and photoluminescence properties of a rare-earth free red-emitting Mn ²⁺ -activated KMgBO ₃ . Dalton Transactions, 2014, 43, 13845-13851.	3.3	67
112	Phase-selective hydrothermal synthesis of Cu ₂ ZnSnS ₄ nanocrystals: the effect of the sulphur precursor. CrystEngComm, 2014, 16, 4306-4313.	2.6	54
113	Preferred orientation of Cu(In,Ga)Se ₂ thin film deposited on stainless steel substrate. Progress in Photovoltaics: Research and Applications, 2013, 21, 838-848.	8.1	8
114	Investigation of Quinquethiophene Derivatives with Different End Groups for High Open Circuit Voltage Solar Cells. Advanced Energy Materials, 2013, 3, 639-646.	19.5	65
115	Structure and photoluminescence properties of KSr_4(BO_3)_3:Eu^3+ red-emitting phosphor. Optical Materials Express, 2012, 2, 92.	3.0	58
116	Structure, morphology and properties of thinned Cu(In, Ga)Se ₂ films and solar cells. Semiconductor Science and Technology, 2012, 27, 035022.	2.0	45
117	Triangle islands and cavities on the surface of evaporated Cu(In, Ga)Se2 absorber layer. Applied Surface Science, 2012, 258, 9747-9750.	6.1	7
118	Luminescence and energy transfer of a color tunable phosphor: Dy3+-, Tm3+-, and Eu3+-coactivated KSr4(BO3)3 for warm white UV LEDs. Journal of Materials Chemistry, 2012, 22, 6463.	6.7	191
119	Controlled synthesis of hierarchical zeolitic imidazolate framework-GIS (ZIF-GIS) architectures. CrystEngComm, 2012, 14, 8280.	2.6	20
120	Effect of Na on lower open circuit voltage of flexible CIGS thin-film solar cells prepared by the low-temperature process. Physica Scripta, 2012, 85, 055806.	2.5	29
121	The role of growth temperature and Se flux on Cu(In,Ga)Se2thin film deposited on a stainless steel substrate and solar cell. Semiconductor Science and Technology, 2012, 27, 065007.	2.0	7
122	Low-temperature preparation of flexible a-Si:H solar cells with hydrogenated nanocrystalline silicon p layer. Vacuum, 2012, 86, 1477-1481.	3.5	6
123	Structural analysis of Cu(In1-xGax)Se2 multi-layer thin film solar cells. Wuli Xuebao/Acta Physica Sinica, 2012, 61, 228801.	0.5	1
124	Research on sodium incorporation methods of growing Cu(In-Ga)Se2 thin film by low-temperature deposition. Wuli Xuebao/Acta Physica Sinica, 2012, 61, 198801.	0.5	0
125	Finite element simulation and experimental research on ZnO:Al by magnetron sputtering. Thin Solid Films, 2011, 520, 887-890.	1.8	1
126	Dynamic scaling and optical properties of Zn(S, O, OH) thin film grown by chemical bath deposition. Chinese Physics B, 2011, 20, 116802.	1.4	1

#	Article	IF	CITATIONS
127	Structural study of nonlinear optical borates K1â^'xNaxSr4(BO3)3 (xâ‰ 0 .5). Powder Diffraction, 2010, 25, S11-S16.	0.2	1
128	Influence of negative ion resputtering on Al-doped ZnO thin films prepared by mid-frequency magnetron sputtering. Applied Surface Science, 2010, 256, 1694-1697.	6.1	35
129	Development of textured back reflector for n–i–p flexible silicon thin film solar cells. Solar Energy Materials and Solar Cells, 2010, 94, 709-714.	6.2	24
130	ZnS thin film deposited with chemical bath deposition process directed by different stirring speeds. Applied Surface Science, 2010, 256, 6871-6875.	6.1	36
131	New Insight into the Role of the Interfacial Molecular Structure on Growth and Scaling in Organic Heterostructures. Journal of Physical Chemistry C, 2010, 114, 13752-13758.	3.1	20
132	CuInSe ₂ Films Prepared by a Plasma-Assisted Selenization Process in Different Working Pressures. Chinese Physics Letters, 2010, 27, 028101.	3.3	5
133	Structure Determination and Relative Properties of Novel Chiral Orthoborate KMgBO ₃ . Inorganic Chemistry, 2010, 49, 2715-2720.	4.0	36
134	Effect of substrate temperature on the structural and electrical properties of CIGS films based on the one-stage co-evaporation process. Semiconductor Science and Technology, 2010, 25, 055007.	2.0	67
135	Experimental Relation between Stranskiâ~'Krastanov Growth of DIP/F ₁₆ CoPc Heterostructures and the Reconstruction of the Organic Interface. Journal of Physical Chemistry C, 2009, 113, 4234-4239.	3.1	26
136	A thermodynamic assessment of the copper–gallium system. Calphad: Computer Coupling of Phase Diagrams and Thermochemistry, 2008, 32, 447-453.	1.6	45
137	Phase relations of the Ag–Ga–N system. Journal of Alloys and Compounds, 2007, 429, 184-191.	5.5	12
138	Subsolidus phase relations of the Cu–Ga–N system. Journal of Alloys and Compounds, 2007, 438, 158-164.	5.5	14
139	Structure Determination of Novel Orthoborate NaMgBO3:  A Promising Birefringent Crystal. Inorganic Chemistry, 2007, 46, 5207-5211.	4.0	58
140	The Na2O–SrO–B2O3 diagram in the B-rich part and the crystal structure of NaSrB5O9. Journal of Solid State Chemistry, 2007, 180, 1470-1475.	2.9	28
141	Thermodynamic assessment of the Ag–Ga system. Calphad: Computer Coupling of Phase Diagrams and Thermochemistry, 2006, 30, 316-322.	1.6	20
142	Crystallographic and magnetic studies on iron-rich mixed rare-earth intermetallics (Nd/Tb)2(Fe/Al)17. Journal of Alloys and Compounds, 2006, 407, 1-7.	5.5	10
143	Influence of rare earth mixing on structural and magnetic properties of Nd2â^'xErxFe17 compounds. Journal of Alloys and Compounds, 2006, 419, 15-20.	5.5	8
144	Thermodynamic analysis of Mg-doped p-type GaN semiconductor. Journal of Alloys and Compounds, 2006, 422, 279-282.	5.5	5

#	Article	IF	CITATIONS
145	Crystal structure and photoluminescence of Tb3+ doped Y3GaO6. Journal of Alloys and Compounds, 2006, 425, 278-283.	5.5	18
146	Crystal structure, magnetic and electrical-transport properties of rare-earth-doped Sr2FeMoO6. Physica B: Condensed Matter, 2006, 381, 233-238.	2.7	29
147	Characterization and photoluminescence of AlN:Eu films. Optical Materials, 2006, 28, 1029-1036.	3.6	19
148	Ab initio structure determination of novel borate NaSrBO3. Journal of Solid State Chemistry, 2006, 179, 1219-1224.	2.9	50
149	Hole doping effects in (Sr2-xNax)FeMoO6 double perovskite. Applied Physics A: Materials Science and Processing, 2006, 84, 459-463.	2.3	8
150	Structure and magnetic phase diagram of mixed rare-earth Nd1â^'xTbxFe10.5Mo1.5 compounds. Journal of Magnetism and Magnetic Materials, 2006, 302, 467-472.	2.3	1
151	Crystal structure and spin reorientation transition of Tb1â^xYxFe11Mo compounds. Journal Physics D: Applied Physics, 2006, 39, 615-620.	2.8	3
152	Visible and infrared emissions from c-axis oriented AlN:Er films grown by magnetron sputtering. Journal of Applied Physics, 2006, 99, 053515.	2.5	16
153	Optical properties of (Y1â~'xTmx)3GaO6 and subsolidus phase relation of Y2O3–Ga2O3–Tm2O3. Journal of Solid State Chemistry, 2005, 178, 1064-1070.	2.9	12
154	Optical spectra of Ln3+(Nd3+, Sm3+, Dy3+, Ho3+, Er3+)-doped Y3GaO6. Journal of Luminescence, 2005, 111, 61-68.	3.1	47
155	Formation, structure and magnetic properties of TbFe12â^'xMox (x=0.5–3.0) compounds. Physica B: Condensed Matter, 2005, 369, 56-63.	2.7	3
156	Structural, magnetic and transport properties of double perovskite compounds (Sr2â^'3xLa2xBax)FeMoO6. Physica B: Condensed Matter, 2005, 370, 228-235.	2.7	17
157	Photoluminescence and characteristics of terbium-doped AlN film prepared by magnetron sputtering. Applied Surface Science, 2005, 245, 391-399.	6.1	9
158	Crystal structure and magnetic properties of Nd1â^'xYxCo6.86Hf0.14 compounds. Journal of Magnetism and Magnetic Materials, 2005, 292, 178-185.	2.3	1
159	Influence of V substitution for Fe on the transport and magnetic properties of Sr2FeMoO6. Solid State Communications, 2005, 133, 223-227.	1.9	15
160	Crystal structure and magnetic properties of Nd1â^'xYxCo6.8Zr0.2 compounds. Journal of Alloys and Compounds, 2005, 394, 69-74.	5.5	2
161	Structures of the ζ and ζ′ phases in the Ag–Ga system. Journal of Alloys and Compounds, 2005, 399, 155-159.	5.5	20
162	Effects of the doping element on crystal structure and magnetic properties of Sm(Co,M)7 compounds (M=Si, Cu, Ti, Zr, and Hf). Intermetallics, 2005, 13, 710-716.	3.9	77

#	Article	IF	CITATIONS
163	Structure and magnetic properties of Mn-doped ZnO nanoparticles. Journal of Applied Physics, 2005, 97, 086106.	2.5	93
164	Crystal structure and magnetic properties of PrCo6.8ÂxCuxHf0.2compounds. Journal Physics D: Applied Physics, 2004, 37, 1881-1884.	2.8	7
165	Effects of iron substitution on magnetic properties of SmCo6.8ÂxFexHf0.2compounds. Journal of Physics Condensed Matter, 2004, 16, 4963-4969.	1.8	4
166	Crystal structure and magnetic properties of SmCo7â^'xHfx compounds. Applied Physics Letters, 2004, 85, 5299-5301.	3.3	57
167	Phase stability, crystal structure, and magnetic properties of NdCo7â^'xHfx compounds. Physica B: Condensed Matter, 2004, 353, 98-103.	2.7	10
168	Crystal structure and magnetic properties of Nd4Ga2O9 and Sm4Ga2O9. Journal of Alloys and Compounds, 2004, 381, 26-31.	5.5	6
169	Optimization of Zn 1– x Sn x O Buffer Layer for Application in CZTSe Solar Cells with H 2 â€Assisted Reactive Sputtering. Physica Status Solidi (A) Applications and Materials Science, 0, , 2100585.	1.8	1